forests

MDPI

Article

A Comparison of Burned Area Time Series in the Alaskan Boreal Forests from Different Remote Sensing Products

José A. Moreno-Ruiz [1], José R. García-Lázaro [1], Manuel Arbelo [2,*] and David Riaño [3,4]

[1] Departamento de Informática, Universidad of Almería, 04120 Almería, Spain; jamoreno@ual.es (J.A.M.-R.); jrgarcia@ual.es (J.R.G.-L.)
[2] Departamento de Física, Universidad de La Laguna, 38200 San Cristóbal de La Laguna, Spain
[3] Instituto de Economía, Geografía y Demografía (IEGD), Centro de Ciencias Humanas y Sociales (CCHS), Consejo Superior de Investigaciones Científicas (CSIC), Albasanz 26-28, 28037 Madrid, Spain; david.riano@cchs.csic.es
[4] Center for Spatial Technologies and Remote Sensing (CSTARS), University of California, 139 Veihmeyer Hall, One Shields Avenue, Davis, CA 95616, USA
* Correspondence: marbelo@ull.es; Tel.: +34-9223182266

Received: 6 March 2019; Accepted: 23 April 2019; Published: 26 April 2019

Abstract: Alaska's boreal region stores large amounts of carbon both in its woodlands and in the grounds that sustain them. Any alteration to the fire system that has naturally regulated the region's ecology for centuries poses a concern regarding global climate change. Satellite-based remote sensors are key to analyzing those spatial and temporal patterns of fire occurrence. This paper compiles four burned area (BA) time series based on remote sensing imagery for the Alaska region between 1982–2015: Burned Areas Boundaries Dataset-Monitoring Trends in Burn Severity (BABD-MTBS) derived from Landsat sensors, Fire Climate Change Initiative (Fire_CCI) (2001–2015) and Moderate-Resolution Imaging Spectroradiometer (MODIS) Direct Broadcast Monthly Burned Area Product (MCD64A1) (2000–2015) with MODIS data, and Burned Area-Long-Term Data Record (BA-LTDR) using Advanced Very High Resolution Radiometer LTDR (AVHRR-LTDR) dataset. All products were analyzed and compared against one another, and their accuracy was assessed through reference data obtained by the Alaskan Fire Service (AFS). The BABD-MTBS product, with the highest spatial resolution (30 m), shows the best overall estimation of BA (81%), however, for the years before 2000 (pre-MODIS era), the BA sensed by this product was only 44.3%, against the 55.5% obtained by the BA-LTDR product with a lower spatial resolution (5 km). In contrast, for the MODIS era (after 2000), BABD-MTBS virtually matches the reference data (98.5%), while the other three time series showed similar results of around 60%. Based on the theoretical limits of their corresponding Pareto boundaries, the lower resolution BA products could be improved, although those based on MODIS data are currently limited by the algorithm's reliance on the active fire MODIS product, with a 1 km nominal spatial resolution. The large inter-annual variation found in the commission and omission errors in this study suggests that for a fair assessment of the accuracy of any BA product, all available reference data for space and time should be considered and should not be carried out by selective sampling.

Keywords: burned area mapping; time series analysis; Alaska; boreal forest; BABD-MTBS; Fire_CCI; MCD64A1; LTDR

1. Introduction

Boreal regions store large quantities of carbon in the vegetation, permafrost, and peatlands that are usually stored for hundreds of years, unless released into the atmosphere by a disturbance (e.g., a wildfire) [1–3]. Any alteration to the fire recurrence patterns and, therefore, to the burned area, could lead to a positive feedback on global climate change as a result of the greenhouse gas emissions that would take place [4]. Alaskan boreal woodlands are not safe from suffering the impact of global warming [5,6]. In the past six decades, Alaska's average temperature has increased by about 3 °F, and models forecast a potential increase of up to an additional 4 °F by 2050 [7]. This rise in the average temperature is causing a modification of the surface energy balance and soil thermal conditions, the exposure of permafrost to thawing due to the decrease in organic soil depth, the decrease in the humidity of forest fuels, the extension of the natural fire season and, therefore, an abnormal spatial and temporal dynamic in these fires.

In order to understand the above changes, it is necessary to have maps of Essential Climate Variables (ECV)—such as the burned area—readily available [8–10]. The georeferenced information must be as exact and consistent as possible and should encompass large periods of time (above 30 years) so that it can be introduced in climate forecast and vegetation dynamics models. The burned area (BA) ECV may be obtained through satellite remote sensing images and have become an important research challenge over the past few decades [11–13].

Multiple remote sensors aboard spatial platforms for the observation of the Earth have been developed in the past 40 years, providing us with a tremendous amount of quality images and data [14]. Processing these images in order to obtain time series of climate variables has involved the use of high-performance computing systems, as well as the development of complex algorithms for their processing [15]. Various burned area products have appeared on the global, continental and regional level, as well as updated versions that include improvements, which have gradually replaced older versions. Amongst these products are the ones developed from daily images of the Moderate Resolution Imaging Spectroradiometer (MODIS) sensor. This sensor has 36 spectral bands with spatial resolutions ranging from 250 m to 1 km. The MCD64A1 C6 (MODIS Direct Broadcast Monthly Burned Area Product Collection 6) product developed by the University of Maryland is currently the official MODIS burned area product globally, with a 500 m spatial resolution [16], while the previous product, the MCD45A1 C5, has been discontinued [17,18]. The ESA (European Spatial Agency) Fire_CCI Project has developed the latest version of the BA product called Fire_CCI 5.1, also based on MODIS images, with a 250 m spatial resolution, which replaces previous versions based on the Medium Resolution Imaging Spectrometer (MERIS) sensor—with a 300 m spatial resolution—that flew aboard the non-operational environmental satellite (ENVISAT) [19]. These two BA products have a temporal coverage limited to the validity period of the MODIS sensor, from the year 2000 onwards. The Advanced Very High-Resolution Radiometer (AVHRR) aboard the NOAA (National Oceanic and Atmospheric Administration) satellites and the various sensors aboard the Landsat satellites, from the Thematic Mapper (TM) aboard the Landsat 5 to Landsat 8's OLI (Operational Land Imager) or the ETM+ (Enhanced TM Plus), are other remote sensors with more temporal coverage used for BA sensing.

AVHRR sensor images have been used in multiple burned area studies as well [20–29]. They are captured daily in five spectral bands and broadcast to the Earth in real time in Local Area Coverage (LAC) format with a 1.1 km spatial resolution. They are also available in a Global Area Coverage (GAC) format with 4.4 km of spatial resolution that is processed aboard the satellite. NASA built the LTDR (Long Term Data Record) [30] dataset—with a spatial resolution of 0.05°—from AVHRR-GAC images, making up the largest available time series of satellite daily images of Earth observation. The University of Almería used this dataset to develop an algorithm based in Bayesian networks for BA mapping in boreal regions [31], which was successfully applied by the researchers to other regions, using other types of images [32,33].

The Landsat-TM/ETM+/OLI sensor has been used in multiple studies of BA sensing at a local and regional level [34–37]. Landsat images are available from the year 1982 and include spectral bands with a high spatial resolution (30 m) but a low temporal resolution (around 16 days). The United States Geological Survey (USGS) has made its Landsat image archive available to the scientific community (https://landsat.usgs.gov/), making it possible to build time series for studies detecting changes in the vegetation cover [38]. Amongst the BA products at a regional level developed from Landsat images time series, two projects funded by the USGS are worth a mention: Monitoring Trends in Burn Severity (MTBS) [39] and Burned Area Essential Climate Variable (BAECV) [40,41], both restricted to the USA—although the latter is currently available only to the Conterminous United States (CONUS)—while products have been announced for Alaska and Uganda.

A significant challenge that all current BA products are posing is the assessment of their accuracy [42,43]. The main difficulties lie in the unavailability of official reference data with which to thoroughly validate them, using higher spatial resolution images instead of the official dataset [11,44]. The bibliography includes frequent comparisons between the various BA products [45], accuracy assessments based on the Pareto boundary [46–50], as well as accuracy assessments based on non-random and very limited samples [51–53]. Few countries have detailed registries of BA perimeters available to use for a full assessment of products resulting from satellite images. The availability of the above information would make it possible to conduct a detailed study of the various products based on the total amount of fires rather than a sample, assess their sensing capabilities, and establish future opportunities for improvement for the algorithms applied.

The post-fire signal is visible for several years in the boreal regions [54], which makes it easier to precisely map the burned area perimeter from satellites. In this study, the Alaskan boreal region—for which a complete reference database including BA perimeters from 1940 compiled by the Alaskan Fire Service (AFS) is available—was selected. The results of this study may be extrapolated to other boreal regions of which there are no reference data. For example, in the boreal region of Siberia, there are no official reference data or available Landsat satellite images in the pre-MODIS era [33], in contrast to a greater number of images after 2000. The launch of Landsat 7, just the year before, considerably increased the probability of obtaining images in high-altitude regions consistently covered by clouds or snowed on. Since then, two Landsat satellites started to operate simultaneously (Landsat 5 and 7).

The main goals of this study are:

1. Building BA time series for the Alaskan boreal forest region from sensors with varying spatial resolutions. The latest versions of the following products available for the Alaska region were considered: BABD-MTBS (30 m), Fire_CCI (250 m), MCD64A1 (500 m), and BA-LTDR (5 km).
2. Calculating the distribution of yearly BA estimations for each product. Conducting a comparison and correlation analysis against the AFS reference data.
3. Assessing the spatial accuracy of the BA products against reference data from metrics resulting from confusion matrices (omission and commission errors).
4. Assessing the theoretical opportunities for improvement in the current BA products through building Pareto boundaries at various spatial resolutions (250 m, 500 m, and 5 km) from reference data.

2. Materials and Methods

2.1. Study Region

The study area is focused around the Alaskan boreal region (Figure 1). Top left-hand corner: (70° N, 168°30′ W); bottom right-hand corner: (60° N, 141° W). The boreal forest takes up over 60% of Alaska's land area, and approximately 43 million ha are covered in woodlands [55]. Prevailing plant species are conifers, primarily black spruce (*Picea mariana* (Mill.) BSP) and white spruce (*Picea glauca* (Moench) Voss), although Balsam poplar (*Populus balsamífera* L.), birch (*Betula neoalaskana* Hook.), and aspen (*Populus tremuloides* Michx.) can also be found in the south-facing sunnier slopes. The rest is

covered in shrubbery, such as willow and highbush cranberry (*Viburnum trilobum* Marsh.), prairies and marshes. This boreal forest is the result of a very cold climate with long winters and very short summers, the presence or absence of permafrost, and forest fires [56].

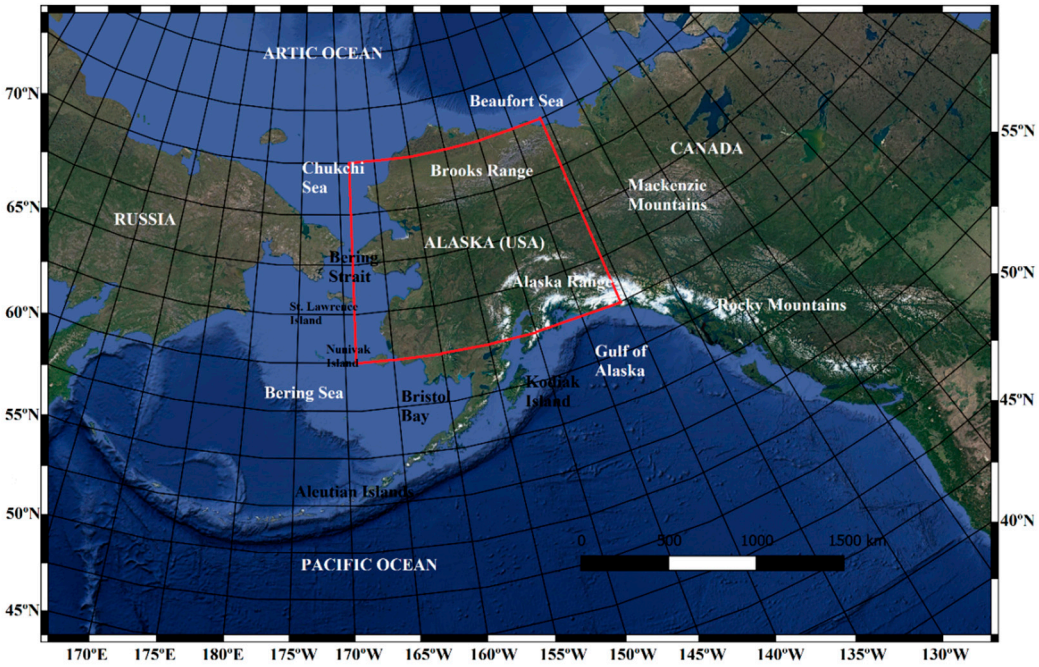

Figure 1. The study region (70° N, 168°30′ W; 60° N, 141° W). Boreal forest (green) is differentiated from all the other land covers (brown) and water bodies (blue).

2.2. *Reference Data*

The Alaskan Fire Service (AFS) maintains a Large Fire Database with fire perimeters recorded in Alaska since 1940 (https://afsmaps.blm.gov/imf/imf.jsp?site=firehistory). It also contains additional fire attribute information (fire name, management office, latitude, longitude, estimated acres, cause, important notes/comments). The data are derived from the best available sources, and metadata include how the fire perimeter was delineated (digitized, GPS or Image Analysis) [57]. Both scale and accuracy may vary across the dataset. For forest fires prior to 1987, fire perimeters of at least 1000 acres (>400 ha) are included. From 1987 onwards, fires with perimeters of at least 100 acres (>40 ha) and, from 1990 onwards, all fires over 10 acres (>4 ha) are included. The database contains 3597 records of fire perimeters until the year 2017—with more than 27 million ha burned and a mean extension of 7538 ha per fire. Large fires of over 10,000 ha have accounted for more than 80% of the total recorded burned area, although they only represent 15% of registered fires (Table 1). Forty-seven very large fires (over 100,000 ha) recorded during this period alone accounted for more than 30% of the total BA. The largest recorded fire (550,000 ha) occurred in 1950.

Table 1. Burned area distribution by fire size in Alaska for 1940 to 2017, as recorded by the Alaska Fire Service (AFS).

Total Burned Area (ha)	**Percentage of Total Burned Area**				
	>100 ha	**>1000 ha**	**>10,000 ha**	**>50,000 ha**	**>100,000 ha**
27,114,076	99.89%	98.24%	82.68%	48.70%	30.68%
Count of Fires	**Percentage of Total fires**				
	>100 ha	**>1000 ha**	**>10,000 ha**	**>50,000 ha**	**>100,000 ha**
3597	77.98%	47.40%	15.04%	3.25%	1.31%

Figure 2 shows the temporal distribution of BA on an annual basis for the 1940–2017 period. The average annual BA was 347,616 ha, but this shows a high variability. Years with a low and even null fire activity alternate with years of very high fire activity—over one million ha burned. The graph highlights the years 2004 (which recorded the largest amount of annual BA, 2.7 million ha) and 2015 (2.1 million ha).

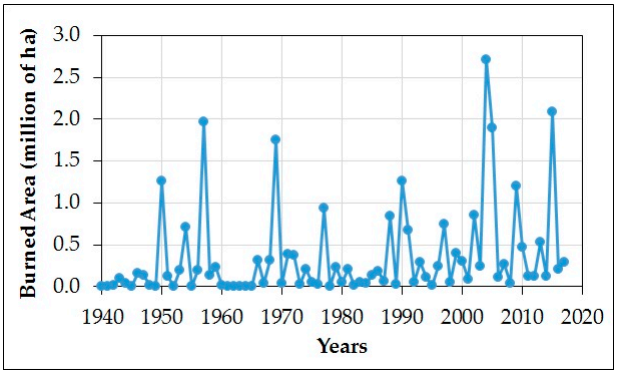

Figure 2. Burned area annual distribution in Alaska for 1940 to 2017, recorded by the Alaska Fire Service (AFS).

All perimeters of fires occurred from 1982 to 2017 were downloaded from AFS and extracted to a shapefile to build annual reference data maps. The vector layers were projected to an Albers Conical Equal Area with a 50 m × 50 m pixel size, using the maximum area method to assign a burned/unburned value [58]. The size of each annual reference map was 29,984 × 38,728 pixels.

2.3. Burned Area Time Series

Four time series were built from four different products of BA generated from satellite images with spatial resolutions ranging from 30 m to 5 km. Table 2 summarizes the main characteristics of these BA products, which are briefly described in the following sections. All annual maps obtained were re-projected to an Albers Conical Equal Area with the same pixel size (50 m) as the reference dataset.

Table 2. Burned area (BA) products analyzed in this study: Burned Areas Boundaries Dataset—Monitoring Trends in Burn Severity (BABD-MTBS), Fire Climate Change Initiative (Fire_CCI) version 5.1, Moderate Resolution Imaging Spectroradiometer (MODIS) Direct Broadcast Monthly Burned Area Product Collection 6 (MCD64A1 C6), and burned area product from Long Term Data Record (BA-LTDR).

BA Product	BABD-MTBS	Fire_CCI 5.1	MCD64A1 C6	BA-LTDR
Coverage	USA	Global	Global	Boreal Region (60° N–70° N)
Time span	1984–2016	2001–2017	2000–present	1982–2015
Sensor	Landsat TM/ETM+/OLI	Terra-MODIS	Terra-MODIS and Aqua-MODIS	NOAA-AVHRR/Terra-MODIS
Spatial resolution	30 m	250 m	500 m	0.05° (~5 km)
Temporal resolution	16 days	Daily	Daily	10 days
Spectral resolution	7/8/11 bands (450–12,500 nm)	15 bands (390–1040 nm)	36 bands (405–14,385 nm)	5 bands (580–12,500 nm)
Reference	[39]	[19]	[16]	[50]

2.3.1. BABD-MTBS

Monitoring Trends in Burn Severity (MTBS) is a joint program between the U.S. Geological Survey Center for Earth Resources Observation and Science (EROS; Sioux Falls, SD, USA) and the USDA Forest Service Geospatial Technology and Applications Center (GTAC; Salt Lake City, UT, USA). MTBS's goal is to map the burn severity and extent of large fires across all lands of the United States from 1984 to the present day. MTBS examines fires of ≥500 acres in the Eastern US and ≥1000 acres in the Western US. The Burned Areas Boundaries Dataset (BABD) is one of the generated products at a 30-meter resolution,

which is freely available to the public as an Environmental Systems Research Institute (ESRI) shapefile (SHP). It includes the perimeters of large fires registered in the CONUS, Alaska, Hawaii, and Puerto Rico in the period spanning from 1984 up until now. BABD data are generated by manual digitalization from the reflectance imagery and the normalized burn ratio (NBR), differenced normalized burn ratio (dNBR) and relativized differenced normalized burn ratio (RdNBR) indexes of a couple of pre- and post-fire Landsat images of fire events recorded from federal and state databases [39].

The BABD-MTBS perimeter data file was downloaded from the project's web server (https://www.mtbs.gov/direct-download), and all fire perimeters in the study region that occurred from 1984 to 2016 were extracted to build the annual burned area maps.

2.3.2. Fire_CCI 5.1

Fire_CCI is one of the 14 parallel projects that comprise the Climate Change Initiative (CCI) of the European Spatial Agency (ESA) to generate ECV data. Its objective is to produce and validate global BA products. Two BA products are distributed as a result of the project, and they are freely available to the public. One of them, the BA Pixel Product version 5.1, covers the period spanning from 2001 to 2017 and is delivered as monthly datasets including the detection date with a 250 m resolution in Georeferenced Tagged Image File Format (GeoTIFF) format [19]. To detect burned pixels, the algorithm uses temporal reflectance changes of the MODIS sensor's red and near-infrared (NIR) bands, combined with thermal information from Collection 6 MODIS active fires/hotspots product [59].

All monthly files corresponding to the geographic subset of North America (area 1) from 2001 to 2017 were downloaded and uncompressed from the ESA server (https://geogra.uah.es/fire_cci/). Layer 1 (date of the first detection) from all files was extracted, resized to the study region and combined on an annual basis in order to build annual burned maps in its native resolution (250 m, lat/long. projection).

2.3.3. MCD64A1 Collection 6

The MCD64A1 Collection 6 is the last version of the MODIS BA Product distributed from Land Processes Distributed Active Archive Center (LP DAAC), based MODIS data from both the Terra and Aqua satellites [16]. The algorithm used to detect burned pixels is based on the Vegetation Index (VI) and active fire observations. VI is built using MODIS short-wave infrared channels 5 and 7: $VI = (\rho 5 - \rho 7)/(\rho 5 + \rho 7)$, where $\rho 5$ and $\rho 7$ are the respective atmospherically corrected surface reflectances. The official product is distributed as monthly files since the year 2000 and is freely available in HDF-EOS format with 5 layers at 500 m (https://e4ftl01.cr.usgs.gov/MOTA/MCD64A1.006/). Also, a re-projected monthly GeoTIFF version covering a set of sub-continental windows is available from the University of Maryland (ftp://ba1.geog.umd.edu). All monthly files corresponding to the window of Alaska (Window 1) from 2000 to 2017 were downloaded and decompressed from the University of Maryland File Transfer Protocol (FTP) server. Band 1 (burn date) from all files was extracted, resized to the study region and combined on an annual basis in order to build annual burned maps in its native resolution (500 m, lat/long. projection).

2.3.4. BA-LTDR

The Burned Area Long-Term Data Record product (BA-LTDR) is based on a Bayesian network algorithm that identifies the potential fire dates for a given year determining the maximum value of the Burned Boreal Forest Index (BBFI) in the 10-day composites LTDR-BSQ files [32]. The algorithm calculates a set of 12 statistical variables based on the surface reflectance and the brightness temperature (AVHRR Channels 1, 2, and 3 for the periods 1982–1999 and 2009–present, and MODIS Channels 1, 2, and 31 for the period 2000–2008) for potential fire dates in the year before a fire event, the year of the event and the year after it. It was originally developed for boreal regions, but it has been successfully applied to other ecosystems and imagery [32,33]. The burned/unburned maps are generated on an annual basis with 5 km resolution and geographic projection for the Alaska region from 1982 to 2015.

2.4. Accuracy Assessment

The temporal accuracy of each BA product has been assessed considering the total calculated annual BA. A timing distribution was represented on a chart, and a correlation analysis of each time series in connection with the reference data for the common period was performed. For the comparison between the different BA products, and, given that not all of them were available before the year 2000, the time series were divided into two periods (pre-MODIS and MODIS).

A detailed analysis of spatial accuracy for each BA product was made based on error matrices versus the reference maps at the pixel level on an annual basis, calculating commission and omission errors of the burned class [60]. Omission errors were calculated as the ratio of burned pixels classified as unburned to the total burned pixels in the BA reference map, while commission errors were calculated as the ratio of unburned pixels classified as burned to the total burned pixels in each BA product under analysis. All products were resampled at 50 m, using the nearest neighbor algorithm, to match the reference and the counts for the error matrices made over those 50 m reference cells.

To minimize the impact of the BA products' georeferencing errors in relation to reference images, each annual image under evaluation was displaced up to 2 pixels from its nominal spatial resolution in all four directions, calculating every corresponding error matrix, and selecting the one with the lowest commission error.

Finally, to estimate if the accuracy of each BA product was limited by its spatial resolution, the Pareto boundaries were analyzed in order to compute the spatial resolution contribution to commission and omission errors [49]. To obtain the Pareto boundary, the BA reference maps were resized to the spatial resolution of each BA product with resampling of aggregated pixels, where each pixel contains a percentage p of burned sub-pixels. For each resized map, a set of $n = 20$ dichotomous maps was constructed considering a pixel as burned on the map i when $p \geq i/n$ ($i = 1, ..., n$) and as not burned otherwise. If the pixel is labelled as burned, the commission error for this pixel is $1 - p$, but if it is labelled as unburned, the omission error is p. For each of these dichotomous maps, the error matrix and the commission (ce) and omission errors (oe) were calculated. The set of commission and omission errors are the points that define the Pareto boundary when they are plotted in a coordinate system (oe/ce). The Pareto boundary represents the minimum omission and commission errors that can be reached at each spatial resolution.

Following Moreno et al. (2014) [50], Pareto boundaries with a 250 m, 500 m and 5 km resolution were computed for each year and for the entire period (1982–2017), using the annual BA reference maps, resized to the corresponding spatial resolutions with pixel aggregate resampling. The distance to the central point of the Pareto boundary was used as an effectiveness measure of the BA product, the lower the better. This central point corresponds to the dichotomous map with a BA value of 50%.

It must be highlighted that MODIS and AVHRR reflectance products used by Fire_CCI 5.1, MCD64A1 C6, and BA-LTDR to create the burned area maps use a nominal pixel size (250/500/5000 m) that does not always match the surface area generated by the reflectance signal detected by the sensor, i.e., the effective spatial resolution. This effective resolution can be much higher, especially for large viewing angles, and particularly evident for high latitudes and for MODIS gridded data [61–64]. In this study, only the nominal spatial resolution of burned area products has been taken into account.

3. Results

3.1. Annual Burned Area Distribution

The total BA computed in the 1982–2017 period with the reference data was approximately 16.81 million ha, with the year 2004 showcasing the highest fire activity (2.71 million ha), while 1995 showed the lowest with only 0.16 million ha burned. Along with the reference data, Figure 3 shows the annual distribution of the total BA in Alaska from 1982 to 2017 for the products under analysis: BABD-MTBS, Fire_CCI 5.1, MCD64A1 C6, and BA-LTDR. The total BA estimate over the period 1984–2015 (the maximum common period for AFS, BABD-MTBS, and BA-LTDR) was 16.25 (100%), 13.12 (80.74%) and

9.04 (55.6%) million ha, respectively. For the pre-MODIS era (1984–1999), AFS estimated 5.12 million ha, BABD-MTBS 2.27 (44.29%) million ha, and BA-LTDR 2.82 (54.94%) million ha. For the MODIS era (2000–2015), AFS considered 11.13 million ha, BABD-MTBS 10.85 (97.52%), Fire_CCI 5.1 7.15 (66.04%), MCD64A1 C6 7.08 (63.63%), and BA-LTDR 6.22 (55.90%) million ha. The correlation coefficient between the annual BA estimates for BABD-MTBS, Fire_CCI 5.1, MCD64A1 C6, and BA-LTDR in relation to the reference data in the time frame for each dataset was 0.95, 0.99, 0.99, and 0.93, respectively. For the pre-MODIS era, the correlation coefficient was 0.80 for BABD-MTBS and 0.94 for BA-LTDR, while for the MODIS era it was 1.00 and 0.93, respectively.

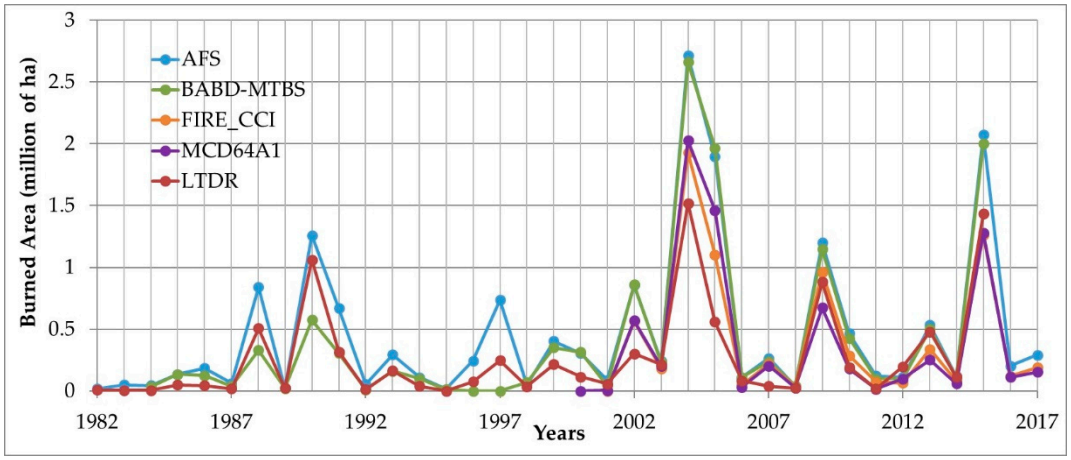

Figure 3. Burned area time series in the Alaskan boreal forests (1982–2017) from the Alaskan Fire Service, Burned Areas Boundaries Dataset - Monitoring Trends in Burn Severity (BABD-MTBS), Fire Climate Change Initiative (Fire_CCI) version 5.1, Moderate Resolution Imaging Spectroradiometer (MODIS) Direct Broadcast Monthly Burned Area Product Collection 6 (MCD64A1 C6), and burned area product from Long Term Data Record (BA-LTDR).

3.2. Spatial Accuracy of the BA Products

Table 3 shows the commission and omission errors resulting from the error matrix for each year and for each BA product. The average commission errors for the BABD-MTBS, Fire_CCI 5.1, MCD64A1 C6, and BA-LTDR products were 0.079, 0.075, 0.178, and 0.290, respectively, whereas the omission errors were 0.256, 0.390, 0.480, and 0.606, respectively. Figure 4 shows the average commission and omission errors for all BA products versus the spatial resolution on a logarithm scale. A linear regression model was computed showing the increase of both types of errors as the spatial resolution worsens.

Table 3. Commission and omission errors by year for the Alaskan boreal region for the Burned Areas Boundaries Dataset-Monitoring Trends in Burn Severity (BABD-MTBS), Fire Climate Change Initiative (Fire_CCI) version 5.1, Moderate Resolution Imaging Spectroradiometer (MODIS) Direct Broadcast Monthly Burned Area Product Collection 6 (MCD64A1 C6), and burned area product from Long Term Data Record (BA-LTDR).

Year	BABD-MTBS		Fire_CCI 5.1		MCD64A1 C6		BA-LTDR	
	Commission Error	Omission Error	Commission Error	Omission Error	Commission Error	Omission Error	Commission Error	Omission Error
1982							1.000	1.000
1983							1.000	1.000
1984	0.095	0.293					1.000	1.000
1985	0.118	0.113					0.334	0.756
1986	0.126	0.407					0.388	0.852
1987	0.291	0.546					0.816	0.946
1988	0.153	0.668					0.146	0.485
1989	0.154	0.233					0.826	0.810
1990	0.113	0.596					0.308	0.417
1991	0.175	0.624					0.354	0.694
1992	0.268	0.847					0.700	0.927
1993	0.068	0.485					0.374	0.652
1994	0.169	0.253					0.473	0.812
1995	0.143	0.324					0.000	1.000
1996	0.000	1.000					0.325	0.794
1997	0.180	1.000					0.143	0.713
1998	0.391	0.123					0.760	0.823
1999	0.105	0.224					0.267	0.608
Subtotal	**0.139**	**0.619**					**0.295**	**0.616**
2000	0.072	0.046			0.000	1.000	0.194	0.697
2001	0.099	0.549	0.303	0.991	1.000	1.000	0.183	0.468
2002	0.092	0.088	0.095	0.402	0.166	0.446	0.167	0.708
2003	0.080	0.114	0.093	0.311	0.386	0.488	0.335	0.410
2004	0.052	0.070	0.064	0.335	0.174	0.383	0.156	0.527
2005	0.094	0.061	0.089	0.47	0.151	0.345	0.256	0.780
2006	0.091	0.082	0.147	0.609	0.424	0.830	0.718	0.782
2007	0.070	0.154	0.155	0.303	0.316	0.476	0.428	0.915
2008	0.246	0.216	0.292	0.438	0.573	0.712	0.326	0.611
2009	0.042	0.083	0.062	0.247	0.094	0.491	0.185	0.400
2010	0.107	0.180	0.11	0.454	0.214	0.697	0.355	0.734
2011	0.059	0.251	0.23	0.543	0.221	0.901	0.270	0.898
2012	0.123	0.225	0.118	0.48	0.516	0.574	0.828	0.695
2013	0.066	0.120	0.055	0.398	0.219	0.631	0.520	0.570
2014	0.017	0.053	0.065	0.35	0.238	0.611	0.870	0.877
2015	0.042	0.075	0.041	0.415	0.155	0.478	0.301	0.516
Subtotal	**0.066**	**0.089**	**0.075**	**0.39**	**0.178**	**0.480**	**0.288**	**0.602**
Total	**0.079**	**0.256**	**0.075**	**0.39**	**0.178**	**0.480**	**0.290**	**0.606**

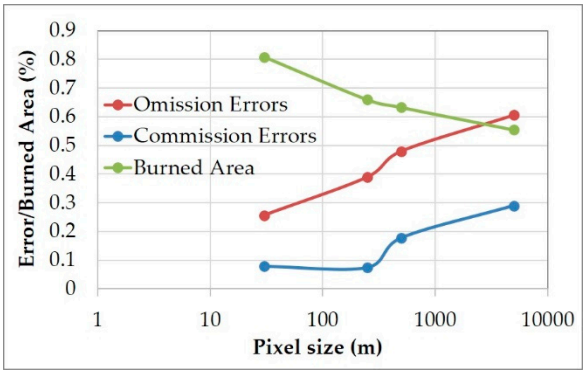

Figure 4. Average percentage of burned area (%) and commission and omission errors (%) versus the spatial resolution (pixel size in meters). The horizontal axis is represented on a log scale.

3.3. Pareto Boundaries of Burned Area Products

Figure 5 shows the average commission/omission errors for each BA product (data from Table 3) in the Alaska region for the study period and their respective Pareto boundaries (250 m, 500 m and

5 km of spatial resolution). The commission/omission errors of BABD-MTBS are closer to its Pareto boundary (50 m, coordinate axis) while commission/omission errors of the other products are farther from its Pareto boundaries (250/500/5000 m). The distance between the point with the average errors and the central point of the Pareto boundary is 0.27, 0.38, 0.47, and 0.37 for BABD-MTBS, Fire_CCI 5.1, MCD64A1 C6, and BA-LTDR, respectively.

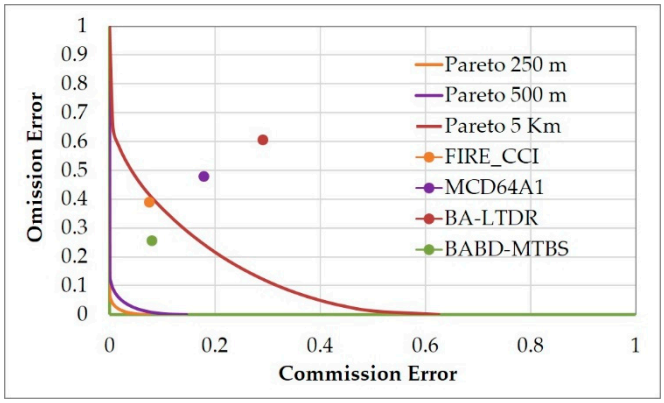

Figure 5. Pareto boundaries (250 m, 500 m and 5 km) of burned area in the Alaska region, and commission and omission errors for the period 1984–2015 for the Burned Areas Boundaries Dataset—Monitoring Trends in Burn Severity (BABD-MTBS), the Fire Climate Change Initiative (Fire_CCI) version 5.1, Moderate Resolution Imaging Spectroradiometer (MODIS) Direct Broadcast Monthly Burned Area Product Collection 6 (MCD64A1 C6), and burned area product from Long Term Data Record (BA-LTDR).

4. Discussion

In a temporal accuracy analysis, all BA time series showed a highly correlated pattern (greater than 90%) with respect to the annual BA reference data. Only the 30 m (BABD-MTBS) and the 5 km (BA-LTDR) time series were available from the 1980s, while the other two start on the year 2000. The fact that, for the period before 2000 (pre-MODIS era), the time series correlation of the BABD-MTBS product with respect to the reference data is significantly lower than for the MODIS era (0.797 vs. 0.999) is remarkable. However, the same is not true for the BA-LTDR product, with a more homogeneous time series correlation value in both periods (0.943 and 0.929). In terms of the estimation of total BA, similar discrepancies were observed in both products. The BABD-MTBS product recorded a high variability between both periods (44.3% versus 97.5%), while BA-LTDR remained almost identical (54.5% and 55.9%). Said inconsistency in the BABD-MTBS product in the pre-MODIS era could be due to the limitation in the number of Landsat images available during that period [65]. The protocol used by BABD-MTBS requires a pair of pre- and post-fire Landsat images, while the sources of the AFS dataset are diverse (digitized, GPS, satellite images).

In the MODIS era, the BABD-MTBS product with the best spatial resolution stands out significantly, virtually matching the reference data in terms of estimation of BA and time series correlation. All remaining products showed results with BA estimates of around 60%. MCD64A1 and Fire_CCI, with detection algorithms using active fires with effective spatial resolutions ranging from 1 km^2 to 10 km^2, obtained similar results in the BA estimation. On the other hand, the fact that BA-LTDR, with a 5km spatial resolution, even matched Fire_CCI and MCD64A1 BA estimations from the year 2009 onwards is noteworthy. The same did not happen from the years 2001 to 2008, a situation that had previously been pointed out by García et al. (2018) [33], because the LTDR dataset used for this period corresponds to version 3 (Continuation), which did not include the brightness temperature of the spectral band of around 3.5–4 μm, which is much more sensitive in burned pixel sensing than the available thermal infrared band between 10.8–11.3 μm [50].

In the spatial accuracy assessment of the estimations, we observed a high relationship between mean commission (ce) and omission (oe) errors versus the spatial resolution logarithm, as well as an

inverse relationship with the burned area percentage. Similar results have previously been measured in a local fire study in Galicia (Northern Spain) in the year 2006 using neuro-fuzzy classifiers at various spatial resolutions [66]. However, it must be noted that this study has used various BA products (each of them based on different images and with different classification algorithms) and has also considered the total recorded fires in the region under study for every year. Generally speaking, we can see an imbalance between commission and omission errors across all products, with the latter being much higher. This translates into an underestimation of the total BA. As we can see in Figure 4, the Fire_CCI product moves away slightly from the linear model in commission errors, whose mean value is similar to that of the BABD-MTBS products, as pointed out before. This causes a bigger imbalance between both errors, which results in a slightly lower BA estimation percentage than would be fitting by spatial resolution. Chuvieco et al. (2018) [19] obtained more balanced global results with the 5.0 de Fire_CCI version (ce = 0.512 and oe = 0.708) for the 2003–2014 period. They used 1200 pairs of pre- and post-fire Landsat images (100 per year) of the whole globe, as well as a sample of official reference perimeters for 4 years, obtaining closer results to those achieved in this study (ce = [0.06–0.29] and oe = [0.27–0.39]) [19]. Meanwhile, Giglio et al. (2018), in a global accuracy assessment of MCD64A1 C6 using a sample of 108 pairs of pre and post-fire Landsat reference scenes non-randomly selected, reported commission and omission errors of 0.24 and 0.37, respectively. Similar results were also reported in the recent study by García et al. (2018) [33] for the north-eastern Siberian region. García et al. (2018) [33] assessed the MCD64A1 (ce = 0.15, oe= 0.23) and BA-LTDR (ce = 0.15, oe = 0.43) products using all burned area perimeters in three chosen years (2002, 2010, and 2011) mapped from 152 pairs of Landsat images.

The detailed analysis in Table 3 points at annual commission/omission errors showing strong fluctuations in connection with mean values, detecting higher errors in certain years. However, the contribution to mean errors for each annual error is weighted by the burned area in said year. This suggests the need to always consider every year in order to obtain the most reliable estimation possible for both errors, and a sampling limited in space and time, as seen in some remote sensing products' assessment protocols, is not recommended [51,52]. It is also noteworthy that, despite the BABD-MTBS showing the best results in terms of average commission and omission errors, the average behavior is very different if the period of study is divided between the pre-MODIS (ce = 0.139, oe = 0.619) and the MODIS (ce = 0.066, oe = 0.089) eras. This result can be primarily explained by the unavailability of Landsat 7 imagery before the year 2000. The same is not true for the BA-LTDR product, which keeps a great consistency without significant differences between both periods, in spite of the problem reported within the period 2001–2008. If the MODIS era is divided into two sub-periods (2001–2008 and 2009–2015), some differences are observed between average commission and omission errors. The 2001–2008 period shows a greater unbalance between both mean errors (ce = 0.214 and oe = 0.652) than the 2009–2015 period (ce = 0.356 and oe = 0.538), thus justifying a greater burned area underestimation in 2001–2008 that is offset by a better estimation of the 2009–2015 sub-period, which matches the pre-MODIS era.

Finally, in this study we have tried to establish the theoretical opportunities for improvement for each one of the BA products, based on their corresponding Pareto boundaries. Pareto boundaries allow us to separate commission and omission errors into two contributions: (1) One due to mixed pixels when using strict classifications in all low spatial resolution products (burned/not burned), (2) the other contribution due to classification errors caused by the limitations of the algorithm and/or the data used in the remote sensing product. Figure 5 shows that average estimations of commission and omission errors are far from the maximum theoretical achievable limit, which means that all BA products under analysis have room for improvement. Using the distance to the central point of the Pareto boundary as a criterion, the MCD64A1 product is the one showing the highest potential for improvement (47%), followed by the Fire_CCI and BA-LTDR (38% and 37%) products, and BABD-MTBS (27%). Note that these results are based on the nominal resolution of the MODIS and AVHRR sensors, however, the effective spatial resolution of the sensors is coarser. Nevertheless, the improvement concept is relative

and depends on the goal we are after. If the aim is to minimize the error in the total BA estimation, the commission and omission errors should be balanced to offset the over and underestimations of BA. For example, out of the four products, the Fire_CCI should slightly decrease the omission error (obviously increasing the commission error at the same time) in order to obtain a better estimation in line with its spatial resolution. The overall improvement of all the above products will gradually happen in the future, not only through the refinement of the very BA remote sensing algorithms but also through the improvement of original image preprocessing (radiometry and geolocation) as well as the use of the ancillary data generated.

5. Conclusions

Four BA time series based on satellite imagery with different spatial resolution, BABD-MTBS (30 m), Fire_CCI (250 m), MCD64A1 (500 m) and BA-LTDR (5 km), were compiled, analyzed and compared with reference data, including BA perimeters from the Alaska Fire Service from 1982 to 2015. For the pre-MODIS era (prior to the year 2000), the product resulting from LTDR images shows the best results in terms of BA estimation. The lack of sufficient Landsat images making it possible to build the time series for the BABD-MTBS 30 m product prevents us from using said data for this period. For that reason, the most reliable source of information for that period would be BA-LTDR. Yet another advantage of BA-LTDR has come to be the consistency that it shows, both in BA estimation percentages and in commission and omission errors in the two periods into which the time series was divided (before and after the year 2000).

Unsurprisingly, given its better spatial resolution, the Landsat-based product is the one showing the best results from the year 2000 onwards, which virtually match the reference data. In that sense, this would mean the BA time series has a higher potential for climate studies from the year 2000. These results also suggest the possibility of using the Landsat data as the reference data—in the absence of official perimeters—in order to assess BA remote sensing algorithms in any other region from the year 2000.

The two products obtained from MODIS data, with detection algorithms dependent, in both cases, on the MODIS (MCD14DL) active fires and thermal anomalies product, show similar results and the best correlation coefficient between the annual burned area estimates in relation to AFS data (0.99). However, Fire_CCI shows an improvement by around 10% with respect to MCD64A1 in commission and omission errors. Based on the theoretical limits of their corresponding Pareto boundaries, they both have significant opportunities for improvement, which are currently limited by the algorithm's reliance on the active fire MODIS product, with a 1 km nominal spatial resolution.

The great year-on-year variation found in the commission and omission errors in this study suggests that the accuracy assessment methodology for any BA product in this or another region must consider all the available reference data for space and time and, whenever possible, should not be carried out by targeted sampling. Accordingly, efforts being made to build time series with Landsat images for other ecosystems will be highly useful for the evaluation and training of algorithms used in other products with better spatial resolution.

Author Contributions: J.R.G.-L. and J.A.M.-R. conceived, designed and applied the methodology. All authors obtained, analyzed and discussed the results; M.A. and D.R. in collaboration with the rest of authors wrote and contributed to the editing of the manuscript.

Funding: This research was funded by the Ministerio de Ciencia, Innovación y Universidades (MCIU), the Agencia Estatal de Investigación (AEI) and the Fondo Europeo de Desarrollo Regional (FEDER) through the project RTI2018-099171-B-I00. The Universidad de La Laguna and the Universidad de Almería partially funded this work through the bridge projects 2018/0001440 and 2019/006, granted in the 2018 and 2019 calls.

Acknowledgments: We wish to thank the three anonymous peer reviewers for their valuable comments and suggestions. The authors also wish to thank the LTDR and MTBS projects and their teams for making the data available, and AFS, NASA, NOAA and USGS for processing and distributing the AFS, MCD64A1 and LTDR datasets. We also thank the ESA Climate Change Initiative and the Fire_CCI project for making the Fire_CCI data available.

Conflicts of Interest: The authors declare no conflict of interest.

References

1. Mann, D.H.; Rupp, T.S.; Olson, M.A.; Duffy, P.A. Is Alaska's Boreal Forest Now Crossing a Major Ecological Threshold? *Arct. Antarct. Alp. Res.* **2012**, *44*, 319–331. [CrossRef]
2. Potter, C. Ecosystem carbon emissions from 2015 forest fires in interior Alaska. *Carbon Balance Manag.* **2018**, *13*. [CrossRef]
3. Chen, G.; Hayes, D.J.; McGuire, A.D. Contributions of wildland fire to terrestrial ecosystem carbon dynamics in North America from 1990 to 2012. *Glob. Biogeochem. Cycles* **2017**, *31*, 878–900. [CrossRef]
4. Mouteva, G.O.; Czimczik, C.I.; Fahrni, S.M.; Wiggins, E.B.; Rogers, B.M.; Veraverbeke, S.; Xu, X.; Santos, G.M.; Henderson, J.; Miller, C.E.; et al. Black carbon aerosol dynamics and isotopic composition in Alaska linked with boreal fire emissions and depth of burn in organic soils. *Glob. Biogeochem. Cycles* **2015**, *29*, 1977–2000. [CrossRef]
5. Kasischke, E.S.; Verbyla, D.L.; Rupp, T.S.; McGuire, A.D.; Murphy, K.A.; Jandt, R.; Barnes, J.L.; Hoy, E.E.; Duffy, P.A.; Calef, M.; et al. Alaska's changing fire regime—Implications for the vulnerability of its boreal forests. *Can. J. For. Res.* **2010**, *40*, 1313–1324. [CrossRef]
6. Kasischke, E.S.; Verbyla, D.L. Fire trends in the Alaskan boreal forest. In *Alaska's Changing Boreal Fororest*; Chapin, F.S., III, Oswood, M.W., Van Cleve, K., Viereck, L.A., Verbyla, D.L., Eds.; Oxford University Press: New York, NY, USA, 2006; pp. 285–301.
7. Melillo, J.M.; Richmond, T.C.; Yohe, G.W. *Climate Change Impacts in the United States: The Third National Climate Assessment*; Chapin, F.S., III, Trainor, S.F., Cochran, P., Huntington, H., Markon, C., McCammon, M., McGuire, A.D., Serreze, M., Eds.; U.S. Global Change Research Program: Washington, DC, USA, 2014; pp. 514–536.
8. Kasischke, E.; Christensen, N.J.; Stocks, B. Fire, global warming, and the carbon balance of boreal forests. *Ecol. Appl.* **1995**, *5*, 437–451. [CrossRef]
9. Van der Werf, G.R.; Randerson, J.T.; Giglio, L.; van Leeuwen, T.T.; Chen, Y.; Rogers, B.M.; Mu, M.; van Marle, M.J.E.; Morton, D.C.; Collatz, G.J.; et al. Global fire emissions estimates during 1997–2016. *Earth Syst. Sci. Data* **2017**, *9*, 697–720. [CrossRef]
10. Yi, K.; Bao, Y. Estimates of wildfire emissions in boreal forests of China. *Fororests* **2016**, *7*, 158. [CrossRef]
11. Chu, T.; Guo, X. Remote sensing techniques in monitoring post-fire effects and patterns of forest recovery in boreal forest regions: A review. *Remote Sens.* **2013**, *6*, 470–520. [CrossRef]
12. Mouillot, F.; Schultz, M.G.; Yue, C.; Cadule, P.; Tansey, K.; Ciais, P.; Chuvieco, E. Ten years of global burned area products from spaceborne remote sensing-A review: Analysis of user needs and recommendations for future developments. *Int. J. Appl. Earth Obs. Geoinf.* **2014**, *26*, 64–79. [CrossRef]
13. Lentile, L.B.; Holden, Z.A.; Smith, A.M.S.; Falkowski, M.J.; Hudak, A.T.; Morgan, P.; Lewis, S.A.; Gessler, P.E.; Benson, N.C. Remote sensing techniques to assess active fire characteristics and post-fire effects. *Int. J. Wildland Fire* **2006**, *15*, 319–345. [CrossRef]
14. Toth, C.; Jóźków, G. Remote sensing platforms and sensors: A survey. *ISPRS J. Photogramm. Remote Sens.* **2016**, *115*, 22–36. [CrossRef]
15. Upadhyay, V.; Kumar, A. Hyperspectral Remote Sensing of Forests: Technological advancements, Opportunities and Challenges. *Earth Sci. Inform.* **2018**, *11*, 487–524. [CrossRef]
16. Giglio, L.; Boschetti, L.; Roy, D.P.; Humber, M.L.; Justice, C.O. The Collection 6 MODIS burned area mapping algorithm and product. *Remote Sens. Environ.* **2018**, *217*, 72–85. [CrossRef] [PubMed]
17. Roy, D.P.; Boschetti, L.; Justice, C.O.; Ju, J. The collection 5 MODIS burned area product—Global evaluation by comparison with the MODIS active fire product. *Remote Sens. Environ.* **2008**, *112*, 3690–3707. [CrossRef]
18. Roy, D.P.; Jin, Y.; Lewis, P.E.; Justice, C.O. Prototyping a global algorithm for systematic fire-affected area mapping using MODIS time series data. *Remote Sens. Environ.* **2005**, *97*, 137–162. [CrossRef]
19. Chuvieco, E.; Lizundia-Loiola, J.; Pettinari, M.L.; Ramo, R.; Padilla, M.; Tansey, K.; Mouillot, F.; Laurent, P.; Storm, T.; Heil, A.; et al. Generation and analysis of a new global burned area product based on MODIS 250 m reflectance bands and thermal anomalies. *Earth Syst. Sci. Data Discuss.* **2018**, 2015–2031. [CrossRef]

20. Barbosa, P.M.; Stroppiana, D.; Grégoire, J.M.; Pereira, J.M.C. An assessment of vegetation fire in Africa (1981–1991): Burned areas, burned biomass, and atmospheric emissions. *Glob. Biogeochem. Cycles* **1999**, *13*, 933–950. [CrossRef]
21. Pereira, J.M.C. A comparative evaluation of NOAA/AVHRR vegetation indexes for burned surface detection and mapping. *IEEE Trans. Geosci. Remote Sens.* **1999**, *37*, 217–226. [CrossRef]
22. Barbosa, P.M.; Grégoire, J.M.; Pereira, J.M.C. An algorithm for extracting burned areas from time series of AVHRR GAC data applied at a continental scale. *Remote Sens. Environ.* **1999**, *69*, 253–263. [CrossRef]
23. Li, Z.; Nadon, S.; Cihlar, J. Satellite-based detection of Canadian boreal forest fires: Development and application of the algorithm. *Int. J. Remote Sens.* **2000**, *21*, 3057–3069. [CrossRef]
24. Kasischke, E.S.; French, N.H.F. Locating and estimating the areal extent of wildfires in alaskan boreal forests using multiple-season AVHRR NDVI composite data. *Remote Sens. Environ.* **1995**, *51*, 263–275. [CrossRef]
25. Sukhinin, A.I.; French, N.H.F.; Kasischke, E.S.; Hewson, J.H.; Soja, A.J.; Csiszar, I.A.; Hyer, E.J.; Loboda, T.; Conrad, S.G.; Romasko, V.I.; et al. AVHRR-based mapping of fires in Russia: New products for fire management and carbon cycle studies. *Remote Sens. Environ.* **2004**, *93*. [CrossRef]
26. Soja, A.J.; Cofer, W.R.; Shugart, H.H.; Sukhinin, A.I.; Stackhouse, P.W.; McRae, D.J.; Conard, S.G. Estimating fire emissions and disparities in boreal Siberia (1998–2002). *J. Geophys. Res. D Atmos.* **2004**, *109*. [CrossRef]
27. Gitas, I.Z.; Mitri, G.H.; Ventura, G. Object-based image classification for burned area mapping of Creus Cape, Spain, using NOAA-AVHRR imagery. *Remote Sens. Environ.* **2004**, *92*, 409–413. [CrossRef]
28. Chuvieco, E.; Englefield, P.; Trishchenko, A.P.; Luo, Y. Generation of long time series of burn area maps of the boreal forest from NOAA-AVHRR composite data. *Remote Sens. Environ.* **2008**, *112*, 2381–2396. [CrossRef]
29. Ponomarev, E.I.; Kharuk, V.I.; Ranson, K.J. Wildfires dynamics in Siberian larch forests. *Forests* **2016**, *7*, 125. [CrossRef]
30. Pedelty, J.; Devadiga, S.; Masuoka, E.; Brown, M.; Pinzon, J.; Tucker, C.; Vermote, E.; Prince, S.; Nagol, J.; Justice, C.; et al. Generating a long-term land data record from the AVHRR and MODIS instruments. *Int. Geosci. Remote Sens. Symp. IGARSS* **2007**, 1021–1024. [CrossRef]
31. Moreno Ruiz, J.A.; Riaño, D.; Arbelo, M.; French, N.H.F.; Ustin, S.L.; Whiting, M.L. Burned area mapping time series in Canada (1984–1999) from NOAA-AVHRR LTDR: A comparison with other remote sensing products and fire perimeters. *Remote Sens. Environ.* **2012**, *117*, 407–414. [CrossRef]
32. Guindos-Rojas, F.; Arbelo, M.; García-Lázaro, J.R.; Moreno-Ruiz, J.A.; Hernández-Leal, P.A. Evaluation of a Bayesian algorithm to detect Burned Areas in the Canary Islands' Dry Woodlands and forests ecoregion using MODIS data. *Remote Sens.* **2018**, *10*, 789. [CrossRef]
33. García-Lázaro, J.R.; Moreno-Ruiz, J.A.; Riaño, D.; Arbelo, M. Estimation of burned area in the Northeastern Siberian boreal forest from a Long-Term Data Record (LTDR) 1982–2015 time series. *Remote Sens.* **2018**, *10*, 940. [CrossRef]
34. Chuvieco, E.; Congalton, R.G. Application of remote sensing and geographic information systems to forest fire hazard mapping. *Remote Sens. Environ.* **1989**, *29*, 147–159. [CrossRef]
35. Díaz-Delgado, R.; Pons, X. Spatial patterns of forest fires in Catalonia (NE of Spain) along the period 1975–1995 analysis of vegetation recovery after fire. *For. Ecol. Manag.* **2001**, *147*, 67–74. [CrossRef]
36. Bastarrika, A.; Chuvieco, E.; Martín, M.P. Mapping burned areas from landsat TM/ETM+ data with a two-phase algorithm: Balancing omission and commission errors. *Remote Sens. Environ.* **2011**, *115*, 1003–1012. [CrossRef]
37. Koutsias, N.; Karteris, M. Burned area mapping using logistic regression modeling of a single post-fire Landsat-5 Thematic Mapper image. *Int. J. Remote Sens.* **2000**, *21*, 673–687. [CrossRef]
38. Zhu, Z. Change detection using landsat time series: A review of frequencies, preprocessing, algorithms, and applications. *ISPRS J. Photogramm. Remote Sens.* **2017**, *130*, 370–384. [CrossRef]
39. Eidenshink, J.; Schwind, B.; Brewer, K.; Zhu, Z.L.; Quayle, B.; Howard, S. A Project for Monitoring Trends in Burn Severity. *Fire Ecol.* **2007**, *3*, 3–21. [CrossRef]
40. Hawbaker, T.J.; Vanderhoof, M.K.; Beal, Y.J.; Takacs, J.D.; Schmidt, G.L.; Falgout, J.T.; Williams, B.; Fairaux, N.M.; Caldwell, M.K.; Picotte, J.J.; et al. Mapping burned areas using dense time-series of Landsat data. *Remote Sens. Environ.* **2017**, *198*, 504–522. [CrossRef]
41. Vanderhoof, M.K.; Fairaux, N.; Beal, Y.J.G.; Hawbaker, T.J. Validation of the USGS Landsat Burned Area Essential Climate Variable (BAECV) across the conterminous United States. *Remote Sens. Environ.* **2017**, *198*, 393–406. [CrossRef]

42. Liu, C.; Frazier, P.; Kumar, L. Comparative assessment of the measures of thematic classification accuracy. *Remote Sens. Environ.* **2007**, *107*, 606–616. [CrossRef]
43. Foody, G.M. Status of land cover classification accuracy assessment. *Remote Sens. Environ.* **2002**, *80*, 185–201. [CrossRef]
44. Belhadj-Khedher, C.; Koutsias, N.; Karamitsou, A.; Ei-Melki, T.; Ouelhazi, B.; Hamdi, A.; Nouri, H.; Mouillot, F. A revised historical fire regime analysis in Tunisia (1985–2010) from a critical analysis of the national fire database and remote sensing. *Forests* **2018**, *9*, 59. [CrossRef]
45. Humber, M.L.; Boschetti, L.; Giglio, L.; Justice, C.O. Spatial and temporal intercomparison of four global burned area products. *Int. J. Digit. Earth* **2019**, *12*, 460–484. [CrossRef]
46. Oliva, P.; Martín, P.; Chuvieco, E. Burned area mapping with MERIS post-fire image. *Int. J. Remote Sens.* **2011**, *32*, 4175–4201. [CrossRef]
47. Anaya, J.A.; Chuvieco, E. Accuracy Assessment of Burned Area Products in the Orinoco Basin. *Photogramm. Eng. Remote Sens.* **2013**, *78*, 53–60. [CrossRef]
48. Mallinis, G.; Koutsias, N. Comparing ten classification methods for burned area mapping in a Mediterranean environment using Landsat TM satellite data. *Int. J. Remote Sens.* **2012**, *33*, 4408–4433. [CrossRef]
49. Boschetti, L.; Flasse, S.P.; Brivio, P.A. Analysis of the conflict between omission and commission in low spatial resolution dichotomic thematic products: The Pareto Boundary. *Remote Sens. Environ.* **2004**, *91*, 280–292. [CrossRef]
50. Moreno-Ruiz, J.A.; García-Lázaro, J.R.; del Águila Cano, I.; Hernández-Leal, P. Burned area mapping in the North American boreal forest using terra-MODIS LTDR (2001–2011): A comparison with the MCD45A1, MCD64A1 and BA GEOLAND-2 products. *Remote Sens.* **2014**, *6*, 815–840. [CrossRef]
51. Boschetti, L.; Stehman, S.V.; Roy, D.P. A stratified random sampling design in space and time for regional to global scale burned area product validation. *Remote Sens. Environ.* **2016**, *186*, 465–478. [CrossRef]
52. Padilla, M.; Stehman, S.V.; Ramo, R.; Corti, D.; Hantson, S.; Oliva, P.; Alonso-Canas, I.; Bradley, A.V.; Tansey, K.; Mota, B.; et al. Comparing the accuracies of remote sensing global burned area products using stratified random sampling and estimation. *Remote Sens. Environ.* **2015**, *160*, 114–121. [CrossRef]
53. Silva, J.M.N.; Sá, A.C.L.; Pereira, J.M.C. Comparison of burned area estimates derived from SPOT-VEGETATION and Landsat ETM+ data in Africa: Influence of spatial pattern and vegetation type. *Remote Sens. Environ.* **2005**, *96*, 188–201. [CrossRef]
54. Moreno-Ruiz, J.A.; Garcia-Lazaro, J.R.; Riano, D.; Kefauver, S.C. The synergy of the 0.05° (~5 km) AVHRR long-term data record (LTDR) and landsat TM archive to map large fires in the North American boreal region from 1984 to 1998. *IEEE J. Sel. Top. Appl. Earth Obs. Remote Sens.* **2014**, *7*, 1157–1166. [CrossRef]
55. Nowacki, G.J.; Spencer, P.; Fleming, M.; Brock, T.; Jorgenson, T. *Unified Ecoregions of Alaska: 2001. U.S. Geological Survey Open-File Report 2002-297*; Geological Survey (U.S.): Reston, VA, USA, 2003. [CrossRef]
56. Chapin, F.S., III; Oswood, M.W.; van Cleve, K.; Viereck, L.A.; Verbyla, D.L. *Alaska's Changing Boreal Forest*; Oxford University Press: New York, NY, USA, 2006.
57. AK Fire History Perimeters. Available online: https://www.arcgis.com/home/item.html?id=d4b8d89f226f4c488e1e4ba054e49be9 (accessed on 23 April 2019).
58. Arnone, E.; Francipane, A.; Scarbaci, A.; Puglisi, C.; Noto, L.V. Effect of raster resolution and polygon-conversion algorithm on landslide susceptibility mapping. *Environ. Model. Softw.* **2016**, *84*, 467–481. [CrossRef]
59. Giglio, L.; Schroeder, W.; Justice, C.O. The collection 6 MODIS active fire detection algorithm and fire products. *Remote Sens. Environ.* **2016**, *178*, 31–41. [CrossRef]
60. Stehman, S.V. Selecting and interpreting measures of thematic classification accuracy. *Remote Sens. Environ.* **1997**, *62*, 77–89. [CrossRef]
61. Hovi, A.; Lindberg, E.; Lang, M.; Arumäe, T.; Peuhkurinen, J.; Sirparanta, S.; Pyankov, S.; Rautiainen, M. Seasonal dynamics of albedo across European boreal forests: Analysis of MODIS albedo and structural metrics from airborne LiDAR. *Remote Sens. Environ.* **2019**, *224*, 365–381. [CrossRef]
62. Wang, Z.; Schaaf, C.B.; Sun, Q.; Shuai, Y.; Román, M.O. Capturing rapid land surface dynamics with Collection V006 MODIS BRDF/NBAR/Albedo (MCD43) products. *Remote Sens. Environ.* **2018**, *207*, 50–64. [CrossRef]

63. Campagnolo, M.L.; Sun, Q.; Liu, Y.; Schaaf, C.; Wang, Z.; Román, M.O. Estimating the effective spatial resolution of the operational BRDF, albedo, and nadir reflectance products from MODIS and VIIRS. *Remote Sens. Environ.* **2016**, *175*, 52–64. [CrossRef]
64. Campagnolo, M.L.; Montano, E.L. Estimation of effective resolution for daily modis gridded surface reflectance products. *IEEE Trans. Geosci. Remote Sens.* **2014**, *52*, 5622–5632. [CrossRef]
65. Egorov, A.; Roy, D.; Zhang, H.; Li, Z.; Yan, L.; Huang, H. Landsat 4, 5 and 7 (1982 to 2017) Analysis Ready Data (ARD) Observation Coverage over the Conterminous United States and Implications for Terrestrial Monitoring. *Remote Sens.* **2019**, *11*, 447. [CrossRef]
66. García Lázaro, J.R.; Ruiz, J.A.M.; Arbelo, M. Effect of spatial resolution on the accuracy of satellite-based fire scar detection in the northwest of the Iberian Peninsula. *Int. J. Remote Sens.* **2013**, *34*, 4736–4753. [CrossRef]